

## Attomolar Detection of Low-Molecular Weight Antibiotics Using Midinfrared-Resonant Toroidal Plasmonic Metachip Technology


Arash Ahmadvand,<sup>1,\*</sup> Burak Gerislioglu<sup>2</sup>, Zeinab Ramezani,<sup>3</sup> and S. Amir Ghoreishi<sup>4</sup>

<sup>1</sup>*Department of Electrical and Computer Engineering, Rice University, 6100 Main St, Houston, Texas 77005, USA*

<sup>2</sup>*Department of Physics and Astronomy, Rice University, 6100 Main St, Houston, Texas 77005, USA*

<sup>3</sup>*Department of Electrical and Computer Engineering, Northeastern University, Boston, Massachusetts 02115, USA*

<sup>4</sup>*Faculty of Electrical & Computer Engineering, Science and Research Branch, Islamic Azad University of Tehran, Tehran, Iran*

 (Received 26 June 2019; revised manuscript received 31 July 2019; published 11 September 2019)

Plasmonic metamaterials can be used to enhance midinfrared sensors and detectors for immunosensing applications. The major challenge with them is to integrate these technologies in low-cost, compact, and promising platforms. As an emerging technique, we utilize toroidal resonant plasmonic metamaterials to develop an ultrasensitive label-free analytical platform for the detection of specific antibiotics in the midinfrared spectra. Taking advantage of the unique sensitivity of robustly squeezed electromagnetic fields in the toroidal plasmonic meta-atoms, we demonstrate that our proposed approach based on toroidal metastructures provides recognition of extremely-low-weight (approximately 0.6 KDa) biological targets at attomolar densities. We envisage that this understanding extends the capabilities of plasmonic metamaterials to analyze the presence of specific biological molecules and organisms with ultrahigh precision.

DOI: [10.1103/PhysRevApplied.12.034018](https://doi.org/10.1103/PhysRevApplied.12.034018)

### I. INTRODUCTION

Plasmonic metachips have revitalized advanced and sensitive label-free biomarker detection techniques by enabling robust electromagnetic field confinement down to extreme subwavelength scales, which has enabled the detection of biomolecules at ultralow densities with high precision [1,2]. This promising counterpart of nanophotonics has promoted the development of cost-effective multianalyte biosensors, tailored for ultrafast and real-time recognition of diverse infection and diseases' fingerprints [1–3]. Considering the hype cycle profile of plasmonic biosensors technology, these devices are currently well into a stable commercialization phase [4]. Plasmonic biosensing devices mostly operate based on the spectral response of resonant nanostructures and are very sensitive to the dielectric materials in contact with the surface of the nanochips. While visible and/or near-infrared wavelength-resonant structures are of particular interest for optic-based pharmacological applications, the midinfrared (mid-IR) band width is particularly well matched for nanometric biomolecule sensorics [5,6]. In general, the mid-IR spectrum encircles the vibrations of most of the biological objects including envelope proteins,

organisms, enzymes, DNA, and lipids [7]. Although the vibration signals of biomolecules are dramatically weak, as a promising technique in accessing these fingerprints, mid-IR spectroscopy facilitates a noninvasive and nondestructive label-free biosensing methodology [8,9]. To this end, resonant plasmonic metamaterials based on artificial building blocks have been extensively exploited for mid-IR biosensing by taking advantage of the displacements in the position of the induced moments due to the variations in the dielectric permittivity of media [8–11]. Traditionally, Fano resonant plasmonic metamaterials have been widely used for mid-IR detection due to showing substantial sensitivity of the induced asymmetric line shape to the environmental perturbations [10,12,13]. In spite of the fact that Fano resonant sensors provide accurate detection of low-weight biological targets at fairly low concentrations, this approach does not efficiently address the identification of ultralow-weight proteins (i.e., beta-amyloid, tau protein) and viruses (i.e., Zika, PRD1, MS2) at the early stage of diseases due to the poor limit of detection (LOD) in practical clinical assays.

Very recently, an alternative class of label-free, on-site, selective, and extremely sensitive plasmonic biosensors has been developed and introduced based on toroidal multipole electrodynamics [14–16]. In the field of theoretical physics, optically driven dynamic toroidal

\*aahmadv@rice.edu

moments constitute an independent group of elementary electromagnetic sources with dramatically weak far-field radiation patterns [17,18]. The fundamental member of toroidal multipoles is a toroidal dipole that can be created by the polarization currents flowing on a surface of a torus along its meridian [17–20]. From a more applied perspective, due to possessing a spectrally narrow response and strongly squeezed local field enhancement, a toroidal dipole manifests higher sensitivity in practical applications. This makes toroidal metamaterials potential alternatives for conventional optical signal transduction mechanisms. This can be better perceived by considering the radiated electric field from the conventional  $[\mathbf{E}_p = \mathbf{n}^2 \mathbf{k}_0^2 (\hat{\mathbf{r}} \times \hat{\mathbf{r}} \times \hat{\mathbf{p}}/r)]$  and toroidal  $[\mathbf{E}_T = \mathbf{n}^3 \mathbf{k}_0^3 (\hat{\mathbf{r}} \times \hat{\mathbf{r}} \times \hat{\mathbf{T}}/r)]$  scatterers, and their relation to the refractive index ( $n$ ) variations of the surrounding media [21]. This feature enables quantitative fingerprinting of extreme subwavelength multimolecular aggregates with remarkable precision that cannot be achieved by existing detection subwavelength systems.

In this work, we demonstrate the attomolar optic-based sensing of ultralow weight (582.6 Da) antibiotic molecules (kanamycin sulfate or Kantrex,  $\text{C}_{18}\text{H}_{36}\text{N}_4\text{O}_{11} \times \text{H}_2\text{SO}_4$ ) using our developed toroidal mid-IR plasmonic metamaterial. The designed metachip consists of judiciously engineered symmetric multipixel gold nanoresonators with the ability to sustain a strong toroidal dipole at the mid-IR spectral range around  $\lambda \sim 5250$  nm ( $\omega \sim 1904.7$   $\text{cm}^{-1}$ ). The preliminary quantitative studies for the refractive index variations (Supplemental Material [25]) verified the unique sensitivity of the system to the minor perturbations in the dielectric properties of the media. As a proof of principle, we detect the presence of Kantrex molecules attached to plasmonic metamolecules at very low concentrations of approximately 600 molecules in 200  $\mu\text{l}$ .

## II. METHODS

### A. Numerical analysis

To accurately predict the plasmonic properties of the proposed toroidal mid-IR metamaterial, we investigate the excitation of the dipolar moment and its interference using the finite-difference time domain (FDTD) method (Lumerical 2019). In our simulations, to extract the plasmonic response of the tailored metastructure, the following parameters are used: The spatial cell sizes are set to 3 nm in all three axes, with 28 perfectly matched layers (PMLs) as the absorptive boundaries. The mid-IR light source is a plane wave with a simulation duration of 600 fs. The dielectric functions for the gold meta-atoms are taken from empirically reported constants by Ordal *et al.* [22]. The current density profile in the Supplemental Material [25] was calculated using the displacement current simulation module based on implementing the effective permittivity of the system ( $\vec{\mathbf{D}} = \epsilon_{\text{eff}} \vec{\mathbf{E}}$ ). Subsequently, the current density

is solved in FDTD simulations via the following equation:  $\vec{\mathbf{J}} = -i\omega(\epsilon_{\text{eff}} - \epsilon_0)\vec{\mathbf{E}}$ . The opposite currents due to opposite magnetic dipoles result in the excitation of a toroidal dipolar ( $\vec{\mathbf{T}}$ ) resonance, which can be described by the right-hand rule (see Supplemental Material [25] for the excitation of the toroidal feature in planar metamolecules) [23,24].

### B. Sample fabrication

The samples are fabricated on a 500- $\mu\text{m}$ -thick quartz substrate using the electron-beam lithography (EBL) technique. The wafers are developed by a PMMA layer and later 3 nm of chromium is deposited on the PMMA layer to enhance conduction. The developed unit cells have a patterned EBL system. Then a 70-nm-thick layer of gold is deposited using an electron beam evaporator with a vacuum pressure of  $6.7 \times 10^{-7}$  Torr. Ultimately, the metallized specimens are immersed in acetone for approximately an hour for liftoff.

### C. Sample preparation and characterization

The fabricated samples covered with kanamycin sulfate solution and the reference substrate are mounted at normal incidence to the incident infrared light. The samples are rinsed thoroughly using deionized water to remove any possible organic substrate contamination, and later dried with a nitrogen gas flow. Once dried, the transmission spectra are measured and evaluated before and after covering with a solution composed of phosphate buffer solution (PBS) and antibiotic molecules (approximately 10  $\mu\text{l}$ ), with an approximate thickness of 5.8 nm. This is done by collecting the transmitted beam using a Fourier-Transform infrared (FTIR) spectrometer (spectral resolution: 0.07  $\text{cm}^{-1}$  and power of up to 190 mW). To prevent atmospheric absorption and remove possible impurities, the data are collected under a dry air expurgate. The thickness of the deposited solution on the samples is defined from ellipsometry measurements.

## III. RESULTS

### A. The spectral response of the plasmonic mid-IR unit cell

First, we analyze the spectral response of the devised plasmonic mid-IR unit cell by considering both numerical and experimental studies. Figure 1(a) illustrates the tailored symmetric plasmonic unit cell with the formation of a spinning closed-loop charge-current configuration around the center of the meta-atom (not to scale). This panel contains the judiciously defined geometries of the unit cell based on FDTD numerical analysis (Methods). A scanning electron microscopy (SEM) image of the fabricated metallic aperture arrays is shown in Fig. 1(b) (for fabrication details, see Sec. II). Considering the mismatch

between the induced magnetic fields and subsequently generated displacement currents ( $\vec{J}$ ) in proximal nanoresonators under a normalized  $y$  polarized beam illumination (Fig. S1, see Supplemental Material for the vectorial surface current density [25]), we validate the excitation of a toroidal dipole feature at  $\lambda \sim 5250$  nm ( $\omega \sim 1904.7$  cm $^{-1}$ ), as shown in Fig. 1(c). In this profile, the blue and orange solid lines explicitly show the numerically and experimentally obtained transmission spectra, respectively, under  $y$  polarized light illumination (solid line). Conversely, for the  $x$  polarized beam (dashed line) excitation, the toroidal feature vanishes due to losing the discrepancy between the circulating magnetic fields and surface current densities in adjacent resonators. To show the influence of the nanosize gaps on the excitation of oppositely rotating magnetic fields ( $\vec{m}$ ) in the unit cell, we depict the distributions of the electric field in a three-dimensional (3D) map in Fig. 1(d). This profile clearly illustrates the intense confinement of plasmons at the capacitive gap spots, which acts as a key parameter in defining the formation of a toroidal dipole [26]. Moreover, the presence and accumulation of proteins, enzymes, molecules, and so on at these capacitive openings dramatically changes the spectral response of a particular metasensor due to affecting the induced magnetic field intensity and spinning properties of the toroidal moment. Our theoretical predictions are confirmed by quantifying the near-field enhancement

around the toroidal structure as a function of operating band width. As plotted in Fig. 1(e), the maximum enhancement of  $|E|^2$  averaged over the meta-atom along the  $z$  axis ( $E_z$ ) occurs at the toroidal dipole wavelength, giving rise to the large spectrally selective enhancement of the plasmonically boosted near field and holds strong promise for biosensing applications.

The nature of the optically driven transmission dip and the scenario to explain the observed spinning moment are explained and represented in the Supplemental Material [25]. In this addendum file and Fig. S2 (see Supplemental Material [25] for the multipolar decomposition), we theoretically calculate the radiated power from the multipoles, verifying the suppression of the electric dipole and simultaneous superposition of magnetic quadrupole and toroidal dipole around the resonance wavelength. The obtained results are consistent with our computations for the displacement current in Fig. S1 (see Supplemental Material [25] for the surface current density). Furthermore, as an alternative route to verify the formation of the head-to-tail toroidal mode, we numerically calculate and plot the cross-sectional ( $x$ - $z$  plane) vectorial magnetic field map for the spinning charge-current configuration in Fig. S3 (see Supplemental Material [25] for the vectorial magnetic field at the cross section). The exhibited graph strongly validates the formation of a head-to-tail toroidal arrangement across the metastructure.

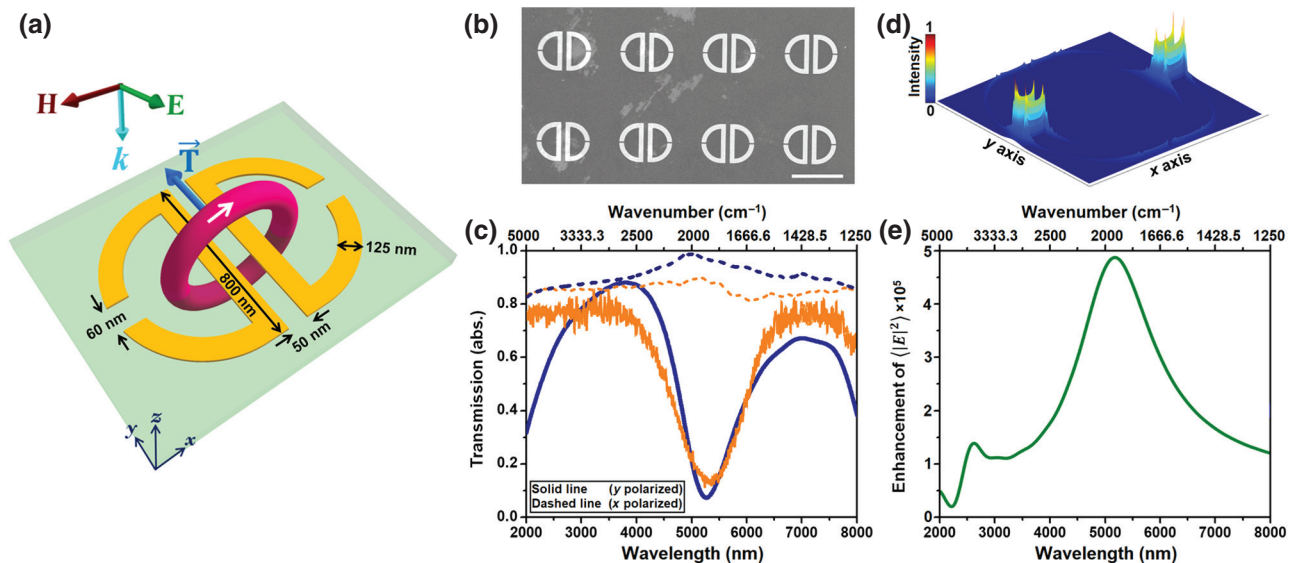


FIG. 1. The spectral response of the toroidal metamaterial. (a) Schematic of the proposed mid-IR plasmonic toroidal meta-atom with the description of the judiciously defined geometries under longitudinal plane wave excitation. The circular spinning feature artificially shows the direction and formation of the head-to-tail charge-current configuration around the unit cell. (b) SEM image of the fabricated metamaterial. The scale base is:  $2 \mu\text{m}$ . (c) Experimentally (orange) and numerically (blue) obtained normalized amplitude transmission spectra for the excitation of toroidal moment under longitudinal (solid) and transverse (dashed) polarization excitations. (d) Three-dimensional (3D) electric field enhancement map for the excitation of the toroidal dipole, showing the strong confinement of plasmons at the capacitive gap spots. (e) Electric field enhancement ( $|E|^2$ ) as a function of incidence, validating significant intensity of the confined fields at the toroidal dipole wavelength.

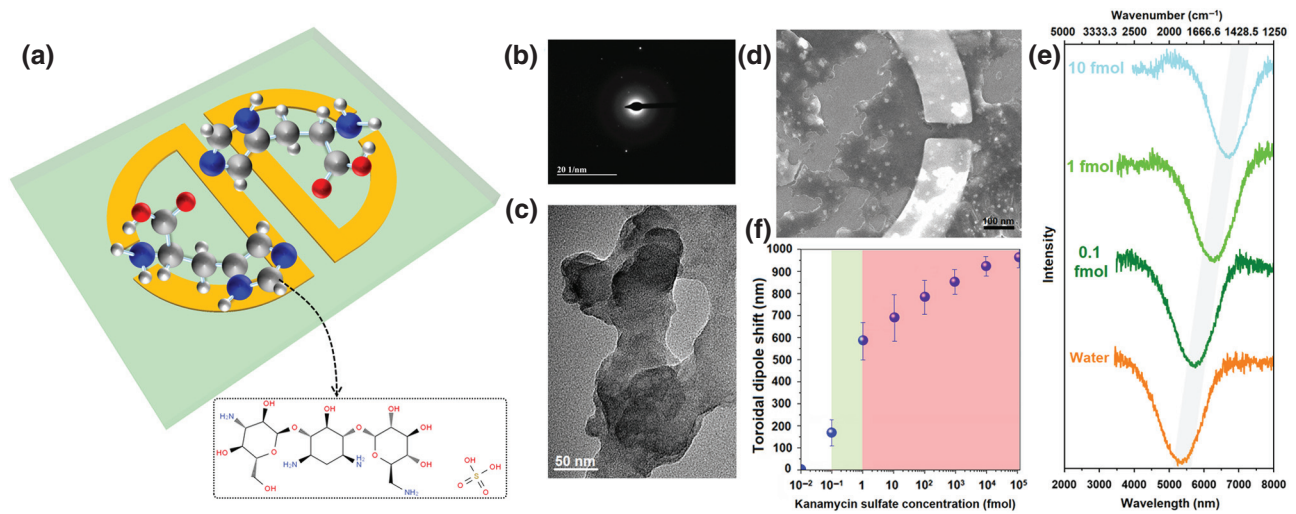


FIG. 2. Principle of biomolecule detection using toroidal plasmonic metamaterial. (a) Schematic of the proposed mid-IR plasmonic toroidal meta-atom with the presence of kanamycin sulfate molecules deposited on the surface. The inset shows the molecular structure for the targeted kanamycin sulfate molecules. (b) Dark- and (c) bright-field images for the diffraction pattern and TEM images of molecules. (d) The SEM image of an area of metamolecule with the presence and accumulation of kanamycin sulfate molecules at the capacitive opening of the metastructure. (e) The experimentally measured transmission spectra for various concentrations of targeted antibiotic molecules. This panel shows a continuous and monotonic redshift in the position of the toroidal dipole by increasing the density of biological objects. (f) Toroidal dipole position value as a function of the kanamycin sulfate molecules' concentration. The shaded red region shows the starting point for the reaction of the toroidal mode to the presence of antibiotic molecules.

### B. Detection of antibiotic molecules by toroidal plasmonic unit cell

The detection performance and sensing properties of the developed mid-IR toroidal metamaterial will now be explained. To verify the sensitivity of the fabricated metamaterials, we qualitatively evaluate the variations in the plasmonic response of the metasensor by varying the refractive index of the medium, as demonstrated in Fig. S4 (see Supplemental Material [25] for the effect of refractive index perturbations). In general, the line shape of a toroidal dipole is very narrow, which allows for a highly accurate measurement of small shifts in resonance wavelength induced by variations in the dielectric permittivity of the unit cell environment [15,16]. Conventionally, the ratio of the plasmonic resonant moment energy shift per refractive index unit perturbation in the surrounding ambience defines the precision of an optical biosensor [27,28]. To explore the sensitivity of the toroidal-resonant meta-atom, we perform a set of experiments by embedding the mid-IR metamaterial in different dielectric liquids (water, acetone, paraldehyde). Figures S4(a) and S4(b) (Supplemental Material [25]) show a substantial and continuous redshift in the position of the toroidal dip by increasing the refractive index of the media  $[(\Delta\lambda_T \sim 950 \text{ nm}) (\Delta\omega_T \sim 304.7 \text{ cm}^{-1}) \text{ for } \Delta n \sim 0.405]$  (see Supplemental Material [25] for the effect of refractive index variations on the spectral response). These significant variations in the toroidal dipole wavelength stem from its higher sensitivity to environmental perturbations. Taking advantage of this

exquisite feature, we utilize the fabricated plasmonic metamaterial for the detection of ultralow weight (approximately 582.6 Da) antibiotic molecules (Kantrex).

Recognition of the presence of these antibiotic molecules around the toroidal meta-atoms is performed by using the transmission difference between two different regimes (the absence and presence of biomolecules) as:  $|\Delta T(\omega) \equiv |t_{yy}^{\text{water}}(\omega)|^2 - |t_{yy}^{\text{molecule}}(\omega)|^2|$ , in which  $t_{yy}$  is the tensor correlating with the transmitted and incident electric fields through the metamaterial under  $y$  polarized light exposure. In Fig. 2(a), an artistic picture of the toroidal unit cell in the presence of a targeted biomolecule is depicted, showing the Kantrex molecules on the metadvice (the inset is the molecular structure of kanamycin sulfate). By mixing the kanamycin sulfate molecules PBS [see the associated dark- and bright-field images for the diffraction pattern and transmission electron microscope (TEM) images of molecules, shown in Figs. 2(b) and 2(c), respectively], we introduce the prepared solution (with approximately  $10 \mu\text{l}$ ) to the plasmonic metamaterial specimens, as shown in the magnified SEM image in Fig. 2(d). The accumulation of Kantrex molecules at the capacitive openings dramatically changes the measured transmission spectra, as shown in Fig. 2(e). Following the same route as the earlier studies in Fig. S4 (see Supplemental Material [25] for the refractive index variations of the media), and considering water as the reference point, we observe a significant redshift in the position of the toroidal dipole in the range of  $5400 \text{ nm} < \lambda_T < 6600 \text{ nm}$

( $1515.1 \text{ cm}^{-1} < \omega_T < 1851.8 \text{ cm}^{-1}$ ), while the concentration of targeted Kantrex molecules continuously increases from 0.1 to 10 fmol. Figure 2(f) shows the toroidal dipole shift as a function of the concentration of Kantrex molecules, where the slope of the redshift of the asymmetric line shape is remarkably sharp from 0.1 to 1 fmol concentrations (green region), and confirms a LOD of approximately 0.85 fmol (850 amol) for the metasensor. This trend is observed for much denser concentrations of kanamycin sulfate molecules with a moderate slope (red region) due to the destructive influence on the formation of toroidal moment, which cancels the mismatch between the rotating magnetic fields and induced surface current densities. To investigate the origin of the resonance shift due to the presence of biomolecules, one should apply both the permittivity variations and near-field coupling in the corresponding computations [29]

$$\frac{\Delta\lambda_T}{\lambda_T} = -\frac{1}{2} \left( \frac{\int_0^t \mathbf{E}_T(\mathbf{r}) \cdot (\hat{\varepsilon} - 1) \cdot \mathbf{E}_T(\mathbf{r}) d\mathbf{r}}{\int_0^\infty |\mathbf{E}_T(\mathbf{r})|^2 d\mathbf{r}} \right) \quad (1)$$

where  $t$  is the thickness of the dropped liquid layer on the surface of the metachip,  $\hat{\varepsilon}$  is the permittivity, and  $|\mathbf{E}_T(\mathbf{r})|$  is the near field at the gaps. It should be emphasized that to introduce the Kantrex molecule to the system, we employ the conversion of its experimentally measured refractive index ( $n = 1.67$ ) to the permittivity. The extrapolated permittivity possesses a nondispersive term ( $n^2$ ), leading to an absorption peak or transmission dip along the mid-IR spectra. In addition, the thickness (approximately 5.8 nm) of the dispersed layer of molecules is defined using the values obtained by ellipsometric data.

Technically,  $\Delta\lambda_T$  possesses a direct influence on the dephasing time and resonant wavelength position of the toroidal metasensor. To exhibit the notion of structure-specific biological detection [30], we consider the dependency of the spectral peak on the wavelength discrepancy between the toroidal resonance moment wavelength and the biological vibrational modes, including the dephasing time of modes, the dipolar mode strength, and bond orientations. Figure 3(a) illustrates the impact on the induced toroidal resonance line shape and the corresponding dephasing time due to the modified transmission tensor. This panel indicates the dephasing time as a function of antibiotic concentration, showing the decay in the toroidal resonance lifetime for both numerically (shaded curve) and experimentally (circles) recorded line shapes (computed by  $\tau = 2\hbar/\text{FWHM}$ ) [31]. Although by increasing the concentration of molecules, the toroidal dipole continuously and monotonically decays, the induced moment reasonably retains its quality for higher concentrations. In Fig. 3(b), we plot the experimental results for before and after the binding of the antibiotic to the metallic meta-atoms, indicating the variations in the transmissivity ratios ( $\Delta T/T$ )

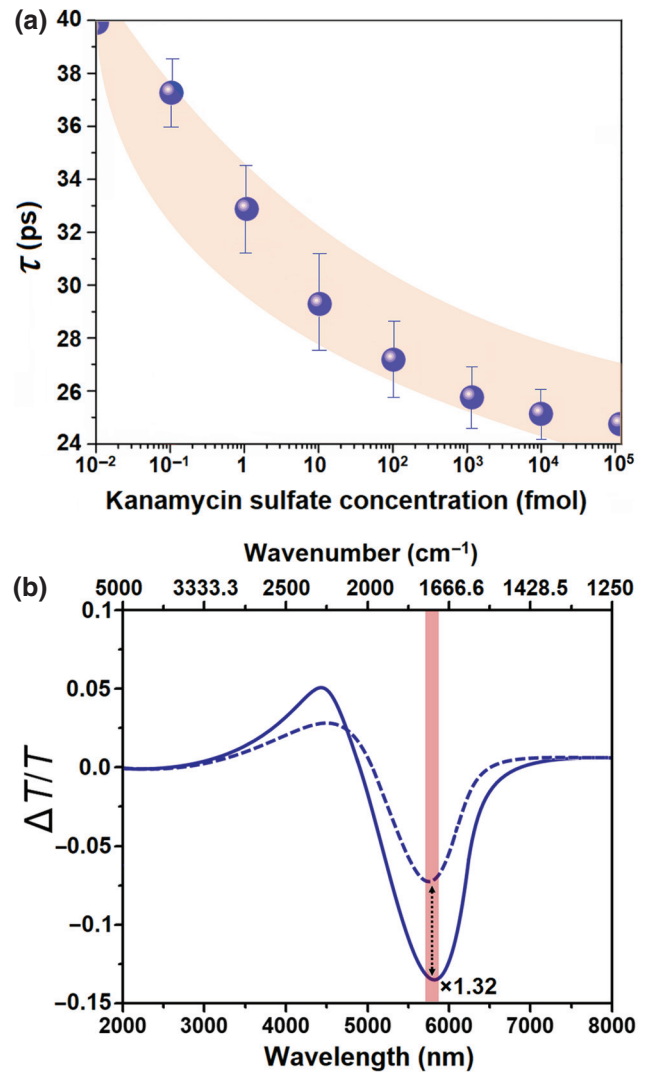


FIG. 3. (a) The lifetime of the toroidal dipole as a function of antibiotic molecules' concentration. (b) Experimentally measured functional change of transmission spectra before (dashed) and after (solid) binding of kanamycin sulfate molecules to the meta-atoms.

of the toroidal moment. Ultimately, Table I compares the LOD and sensitivity of the recently proposed trending mid-IR biosensing technologies with the current study. Noticeably, the proposed approach in this context provides a remarkable detection performance due to taking advantage of strong electromagnetic field confinement by the toroidal dipole, allowing to access attomolar concentrations of the targeted molecule.

#### IV. DISCUSSION

Here, we first conduct a numerical refractive index sensing analysis, as a proof of principle, to demonstrate the enhanced sensitivity of the tailored mid-IR metasensor. The detection of ultralow-weight molecules at extremely

TABLE I. Comparison of the current toroidal plasmonic metasensor performance with those of other mid-IR plasmonic biosensors.

Sensing mechanism	Targeted object	Sensitivity	Limit of detection	Ref.
Gold island functionalized chalcogenide films	Pathogens	...	$10^3$ cfu/ml	[7]
All-semiconductor plasmonic gratings	Dispersionless material	$\sim 900 \pm 20$ nm/r.i.u.	...	[32]
Graphene-mediated hybrid metamaterial	Glucose	...	200 pM (36 pg/ml)	[9]
Nanoplasmonic structure	Amide I/Monomers/Fibrils and Oligomers	220 nm/ r.i.u.	...	[33]
Gold nanoantenna array	Glucose and fructose solutions	10 g/l	55 mM	[34]
Graphene-mediated hybrid metamaterial	Secondary structure of protein immunoglobulin (IgG)	...	30 pM	[35]
Toroidal plasmonic metasensor	Kanamycin sulfate	$\sim 2500$ nm/r.i.u.	850 amol	Current study

low densities is the most important advantage of the toroidal metasensor. Although the conventional resonant subwavelength structures, such as Fano and electromagnetically induced transparency resonant plasmonic sensors, are famous for supporting ultrasharp resonances, and enhanced FOMs and sensitivities, they fail in detecting molecules at extremely low-level concentrations (e.g., amol, fmol, etc.). The proposed approach in this understanding bridges this gap in the field of plasmonic biosensing via toroidal metastructure technology. In addition, the influence of the capacitive gaps is another vital parameter with which to precisely address this. We employ the direct coating of the solution on the surface of the specimens similar to the method developed by Ref. [36]. As depicted in the SEM image in Fig. 2(d), we observe the biological targets at the capacitive openings. Then the control experiments are done by changing the concentration of kanamycin sulfate in the solution between 0.1 to 10 fmol to monitor the effect of the density of the molecules on the plasmonic response. Given that the coating process is performed by introducing the molecules to the substrate, we do expect to have a nonuniform distribution of molecules on the samples.

## V. CONCLUSION

In conclusion, we demonstrate an alternative application of toroidal resonant plasmonic metamaterial to detect ultralow-weight antibiotic molecules at attomolar concentrations along the mid-IR spectra. As a proof of principle, we obtain detection of Kantrex molecules with significant LOD down to 0.85 fmol. By validating the excitation of toroidal dipoles in the mid-IR band, we

qualitatively investigate the sensing performance of the tailored metasensor for several concentrations of the targeted biological molecules. The significant LOD of the developed metadevices stems from the remarkable sensitivity of toroidal meta-atoms to the minor variations in the dielectric permittivity of the media. We envision that the proposed toroidal metasensor technology possesses strong potential to be employed for practical and modern on-chip biosensing applications.

## ACKNOWLEDGMENTS

The authors acknowledge the Ellipsometry and FTIR measurements of the samples by the facility in Islamic Azad University, Iran.

A.A. and B.G. equally contributed to the work presented in this article.

- 
- [1] A. G. Brolo, Plasmonics for future biosensors, *Nat. Photon* **6**, 709 (2012).
  - [2] B. Špačková, P. Wrobel, M. Bocková, and J. Homola, Optical biosensors based on plasmonic nanostructures: A review, *Proc. IEEE* **104**, 2380 (2016).
  - [3] Y. Liu, S. Chen, Q. Liu, J. F. Masson, and W. Peng, Compact multi-channel surface plasmon resonance sensor for real-time multi-analyte biosensing, *Opt. Express* **23**, 20540 (2015).
  - [4] S. M. Yoo and S. Y. Lee, Optical biosensors for the detection of pathogenic microorganisms, *Trends Biotechnol.* **34**, 7 (2016).
  - [5] T. Low and P. Avouris, Graphene plasmonics for terahertz to mid-infrared applications, *ACS Nano* **8**, 1086 (2014).

- [6] Y. T. Chang, Y. C. Lai, C. T. Li, C. K. Chen, and T. J. Yen, A multi-functional plasmonic biosensor, *Opt. Express* **18**, 9561 (2010).
- [7] C. Yu, A. Ganjoo, H. Jain, C. G. Pantano, and J. Irudayaraj, Mid-IR biosensor: Detection and fingerprinting of pathogens on gold island functionalized chalcogenide films, *Anal. Chem.* **78**, 2500 (2006).
- [8] S. Law, L. Yu, A. Rosenberg, and D. Wasserman, All-semiconductor plasmonic nanoantennas for infrared sensing, *Nano Lett.* **13**, 4569 (2013).
- [9] Y. Zhu, Z. Li, Z. Hao, C. DiMarco, P. Maturavongsadit, Y. Hao, M. Lu, A. Stein, Q. Wang, J. Hone, and N. Yu, Optical conductivity-based ultrasensitive mid-infrared biosensing on a hybrid metasurface, *Light Sci. Appl.* **7**, 67 (2018).
- [10] A. B. Khanikaev, C. Wu, and G. Shvets, Fano-resonant metamaterials and their applications, *Nanophotonics* **2**, 247 (2013).
- [11] N. Liu and A. Pucci, Plasmonic biosensors: Know your molecules, *Nat. Mater.* **11**, 9 (2012).
- [12] S. H. Mousavi, I. Kholmanov, K. B. Alici, D. Purtseladze, N. Arju, K. Tatar, D. Y. Fozdar, J. W. Suk, Y. Hao, A. B. Khanikaev, and R. S. Ruoff, Inductive tuning of Fano-resonant metasurfaces using plasmonic response of graphene in the mid-infrared, *Nano Lett.* **13**, 1111 (2013).
- [13] Z. Geng, X. Zhang, Z. Fan, X. Lv, and H. Chen, A route to terahertz metamaterial biosensor integrated with microfluidics for liver cancer biomarker testing in early stage, *Sci. Rep.* **7**, 16378 (2017).
- [14] A. Ahmadvand, B. Gerislioglu, R. Ahuja, and Y. K. Mishra, Terahertz plasmonics: The rise of toroidal metadevices towards immunobiosensings, *Mater. Today*. To be published (2019).
- [15] A. Ahmadvand, B. Gerislioglu, P. Manickam, A. Kaushik, S. Bhansali, M. Nair, and N. Pala, Rapid detection of infectious envelope proteins by magnetoplasmonic toroidal metasensors, *ACS Sens.* **2**, 1359 (2017).
- [16] A. Ahmadvand, B. Gerislioglu, A. Tomitaka, P. Manickam, A. Kaushik, S. Bhansali, M. Nair, and N. Pala, Extreme sensitive metasensor for targeted biomarkers identification using colloidal nanoparticles-integrated plasmonic unit cells, *Biomed. Opt. Express* **9**, 373 (2018).
- [17] B. Gerislioglu and A. Ahmadvand, The observation of high-order charge-current configurations in plasmonic meta-atoms: A numerical approach, *Photonics* **6**, 43 (2019).
- [18] N. Papasimakis, V. A. Fedotov, V. Savinov, T. A. Raybould, and N. I. Zheludev, Electromagnetic toroidal excitations in matter and free space, *Nat. Mater.* **15**, 263 (2016).
- [19] T. Kaelberer, V. A. Fedotov, N. Papasimakis, D. P. Tsai, and N. I. Zheludev, Toroidal dipolar response in a metamaterial, *Science* **330**, 1510 (2010).
- [20] S. Xu, A. Sayanskiy, A. S. Kupriianov, V. R. Tuz, P. Kapitanova, H. B. Sun, W. Han, and Y. S. Kivshar, Experimental observation of toroidal dipole modes in all-dielectric metasurfaces, *Adv. Opt. Mater.* **7**, 1801166 (2019).
- [21] A. Ahmadvand, Ph.D. dissertation, Florida International University, 2018.
- [22] M. A. Ordal, R. J. Bell, R. W. Alexander, L. L. Long, and M. R. Querry, Optical properties of Au, Ni, and Pb at submillimeter wavelengths, *Appl. Opt.* **26**, 744 (1987).
- [23] M. Gupta and R. Singh, Toroidal versus Fano resonances in high Q planar THz metamaterials, *Adv. Opt. Mater.* **4**, 2119 (2016).
- [24] Z. Liu, S. Du, A. Cui, Z. Li, Y. Fan, S. Chen, W. Li, J. Li, and C. Gu, High-quality-factor mid-infrared toroidal excitation in folded 3D metamaterials, *Adv. Mater.* **29**, 1606298 (2017).
- [25] See Supplemental Material at <http://link.aps.org/supplemental/10.1103/PhysRevApplied.12.034018> for details.
- [26] A. Ahmadvand and B. Gerislioglu, Directional toroidal dipoles driven by oblique poloidal and loop current flows in plasmonic meta-atoms, *J. Phys. Chem. C* **122**, 24304 (2018).
- [27] L. J. Sherry, S. H. Chang, G. C. Schatz, R. P. Van Duyne, B. J. Wiley, and Y. Xia, Localized surface plasmon resonance spectroscopy of single silver nanocubes, *Nano Lett.* **5**, 2034 (2005).
- [28] K. M. Mayer and J. H. Hafner, Localized surface plasmon resonance sensors, *Chem. Rev.* **111**, 3828 (2011).
- [29] J. D. Joannopoulos, S. G. Johnson, J. N. Winn, and R. D. Meade, *Photonic Crystals: Molding the Flow of Light* (Princeton Univ. Press, New Jersey, 2008).
- [30] B. R. Eggins, *Biosensors: An Introduction* (Springer-Verlag, New York, 2013).
- [31] A. Ahmadvand, B. Gerislioglu, and Z. Ramezani, Gated graphene islands enabled tunable charge transfer plasmon terahertz metamodulator, *Nanoscale* **11**, 8091 (2019).
- [32] F. B. Barho, F. Gonzalez-Posada, M.-J. Milla-Rodrigo, M. Bomers, L. Cerutti, and T. Taliercio, All-semiconductor plasmonic gratings for biosensing applications in the mid-infrared spectral range, *Opt. Express* **24**, 16175 (2016).
- [33] D. Etezadi, J. B. Warner, IV, F. S. Ruggeri, G. Dietler, H. A. Lashuel, and H. Altug, Nanoplasmonic mid-infrared biosensor for in vitro protein secondary structure detection, *Light Sci. Appl.* **6**, e17029 (2017).
- [34] L. Kuhner, R. Semenyshyn, M. Hentschel, F. Neubrech, C. Tarin, and H. Giessen, Vibrational sensing using infrared nanoantennas: Toward the noninvasive quantitation of physiological levels of glucose and fructose, *ACS Sens.* **4**, 1973 (2019).
- [35] Z. Li, Y. Zhu, Y. Hao, M. Gao, M. Lu, A. Stein, A.-H. A. Park, J. C. Hone, Q. Lin, and N. Yu, Hybrid metasurface-based mid-infrared biosensor for simultaneous quantification and identification of monolayer protein, *ACS Photonics* **6**, 501 (2019).
- [36] L. Xie, W. Gao, J. Shu, Y. Ying, and J. Kono, Extraordinary sensitivity enhancement by metasurfaces in terahertz detection of antibiotics, *Sci. Rep.* **5**, 8671 (2015).